UCSF
UC San Francisco Previously Published Works

Title

Intra-myocardial alginate hydrogel injection acts as a left ventricular mid-wall constraint in swine

Permalink

https://escholarship.org/uc/item/1r40c721

Authors

Sack, Kevin L
Aliotta, Eric
Choy, Jenny S
et al.

Publication Date

2020-07-01

DOI

10.1016/j.actbio.2020.04.033

Peer reviewed

eScholarship.org Powered by the California Digital Library
University of California

Author Manuscript

Author Manuscript

Author Manuscript

Author Manuscript

HHS Public Access

Author manuscript

Acta Biomater. Author manuscript; available in PMC 2021 July 15.

Published in final edited form as:

Acta Biomater. 2020 July 15; 111: 170–180. doi:10.1016/j.actbio.2020.04.033.

Intra-myocardial alginate hydrogel injection acts as a left ventricular mid-wall constraint in swine

Kevin L. Sack[a,b], **Eric Aliotta**[c], **Jenny S. Choy**[d], **Daniel B. Ennis**[c], **Neil H. Davies**[f], **Thomas Franz**[b,e], **Ghassan S. Kassab**[d], **Julius M. Guccione**[a,*]

[a]Division of Adult Cardiothoracic Surgery, Department of Surgery, University of California at San Francisco, Box 0118, UC Hall Room U-158, San Francisco, CA, United States

[b]Division of Biomedical Engineering, Department of Human Biology, University of Cape Town, Cape Town, South Africa

[c]Department of Radiological Sciences, University of California, Los Angeles, California, USA

[d]California Medical Innovations Institute, Inc., San Diego, California, USA

[e]Bioengineering Science Research Group, Engineering Sciences, Faculty of Engineering and the Environment, University of Southampton, Southampton, UK

[f]Cardiovascular Research Unit, Department of Surgery, University of Cape Town, Cape Town, South Africa

Abstract

Despite positive initial outcomes emerging from preclinical and early clinical investigation of alginate hydrogel injection therapy as a treatment for heart failure, the lack of knowledge about the mechanism of action remains a major shortcoming that limits the efficacy of treatment design. To identify the mechanism of action, we examined previously unobtainable measurements of cardiac function from *in vivo, ex vivo*, and *in silico* states of clinically relevant heart failure (HF) in large animals. High-resolution *ex vivo* magnetic resonance imaging and histological data were used along with state-of-the-art subject-specific computational model simulations. *Ex vivo* data were incorporated in detailed geometric computational models for swine hearts in health ($n = 5$), ischemic HF ($n = 5$), and ischemic HF treated with alginate hydrogel injection therapy ($n = 5$). Hydrogel injection therapy mitigated elongation of sarcomere lengths (1.68 ± 0.10 μm [treated] vs. 1.78 ± 0.15 μm [untreated], $p < 0.001$). Systolic contractility in treated animals improved substantially (ejection fraction = 43.9 ± 2.8% [treated] vs. 34.7 ± 2.7% [untreated], $p < 0.01$). The *in silico* models realistically simulated *in vivo* function with >99% accuracy and predicted small myofiber strain in the vicinity of the solidified hydrogel that was sustained for up to 13 mm away from the implant. These findings suggest that the solidified alginate hydrogel material acts as an

*Corresponding author. julius.guccione@ucsf.edu (J.M. Guccione).

Disclosures

KS, EA, JSC, DBE, ND, TF and GSK have nothing to disclose. JMG has served as a consultant for Dassault Systemes, Inc.

Supplementary materials

Supplementary material associated with this article can be found, in the online version, at doi: doi:10.1016/j.actbio.2020.04.033.

Author Manuscript Author Manuscript Author Manuscript Author Manuscript

LV mid-wall constraint that significantly reduces adverse LV remodeling compared to untreated HF controls without causing negative secondary outcomes to cardiac function.

Keywords

Heart failure; Remodeling; Computational modeling; Hydrogel injection therapy

1. Introduction

There is considerable interest in intra-myocardial hydrogel injections as a treatment for heart failure (HF). Ischemic heart disease has a high prevalence and remains the leading cause of mortality worldwide [1]. In the US alone, 550,000 new incidents of myocardial infarction (MI) occur annually [2] and many patients experience post-MI adverse left ventricular (LV) remodeling, which manifests as progressive changes in LV structure and function. Post-MI LV remodeling accounts for nearly 70% of all HF cases [3].For end-stage HF, heart transplantation or mechanical assist devices are the only viable options [4, 5].The opportunity for heart transplantation is limited due to the scarcity of donor organs (3000 per year) relative to the number of potential transplant recipients (70,000 per year). Therefore, the search for new therapies is a critical priority.

The progressive pathological changes after MI are challenging to overcome. The loss of cardiomyocytes and degradation of the LV extracellular matrix lead to wall thinning, infarct expansion at the border-zone [6], scar tissue formation, and eventual LV dilation (accompanied by increased stress). Collectively, these changes induce negative cascading effects on the size, shape and functional performance of the LV [7].The prevention of further LV dilation and adverse remodeling has been the principal target of HF treatment for decades. Numerous pharmacological and device interventions have been designed to achieve this, yet most only address symptomatic and clinical benefit [8, 9].

Injectable hydrogels have shown promise in pre-clinical studies, resulting in improvements including increased ventricular wall thickness [10–15], increased scar thickness [11, 14–16], higher ejection fractions (EFs) [10, 11, 13, 15–17] and decreased ventricular dilation [10–14, 16].Patients with HF treated with an injectable alginate hydrogel and coronary artery bypass-grafting (CABG) also showed improvements in EF, decreased ventricular wall stress, and increased wall thickness three and six months after treatment [18].Additionally, HF patients enrolled in clinical trials of injectable alginate hydrogel experienced significant improvement in New York Heart Association (NYHA) functional class description, mean peak VO2 and quality of life [19, 20].While these positive outcomes illustrate the potential of hydrogel injections as an emerging therapy for HF, the mechanism of action underlying the therapy remains unclear. This shortfall in knowledge limits the ability of translational research to modify therapy protocols to maximize potential efficacy.

The objective of this study was to determine the mechanism of action of inert intra-myocardial hydrogel implants used in a recent clinical trial [20].It should be noted that non-inert biopolymers (e.g., fibrin, hyaluronic acid-based, extracellular matrix-derived materials,

Author Manuscript Author Manuscript Author Manuscript Author Manuscript

etc.) induce a combination of complex mechanical, physiological and chemical signaling mechanisms that cannot be separated as easily as an inert material.

To accomplish our objective, we used a previously validated computational modeling framework [21] that replicated *in vivo* functional performance at resolutions only possible with *ex vivo* imaging, thus providing highly detailed "virtual" hearts that illuminate the hydrogel's mechanism of action. Accordingly, we created 15 subject-specific swine heart computational models in healthy ($n = 5$), diseased ($n = 5$), and treated states ($n = 5$). The mechanical analysis of these models, contextualized by our prior findings [15, 21, 22] and combined with new histological sampling, elucidated the mechanism of action of intra-myocardial hydrogel injection therapy. These findings showed that the solidified hydrogel acted as an LV mid-wall constraint (Fig. 1), which effectively prevented adverse remodeling in the heart without having negative secondary effects on cardiac function.

2. Methods

2.1. Experimental protocol

The experimental protocol was approved by the California Medical Innovations Institute's Institutional Animal Care and Use Committee, and in compliance with the "Guide for the Care and Use of Laboratory Animals" prepared by the Institute of Laboratory Animal Resources, National Research Council, and published by the National Academy Press, revised 1996. Ten domestic swine with HF and five normal healthy swine were divided into groups according to treatment as follows: Normal control (NC) swine that served as a control ($n = 5$); heart-failure injected (HFI) swine that received hydrogel injections ($n = 5$), and heart-failure control (HFC) swine that served as control ($n = 5$). Details about these animals and the creation of HF have been described previously [15].

In brief, branches of the left circumflex artery (the left marginal artery and the posterolateral artery) were occluded via percutaneous placement of embolization coils using a microcatheter (Cantata 2.9, Cook Medical, Bloomington, IN). This creates a realistic model of ischemic cardiomyopathy highly translational to the clinical presentation of HF. Induced MI resulted in ischemia and a steady decline of EF from $>50\%$ at time of occlusion to $<40\%$ eight weeks later. The swine designated for treatment received hydrogel injection therapy eight weeks into their recovery. Control subjects recovered without any intervention. The treated group had alginate hydrogel (LoneStar Heart Inc. Laguna Hills, CA) directly injected in a circumferential pattern into the LV free wall during an open chest procedure. A total of 12–14 injections (0.3 mL each) were administered in two rows: one above and one below the mid-ventricular plane between the base and the apex. Imaging and reconstruction of the injection pattern in a typical treated heart are provided in supplementary Fig. S1. The hydrogel solidifies shortly after injection with a stiffness similar to that of passive myocardium [23].At 16 weeks from initiation of ischemia all HF swine were sacrificed, at which time excised hearts were fixed with buffered formalin (Carson-Millonig formulation). Details about how the hearts were studied with high-resolution *ex vivo* magnetic resonance imaging (MRI) have been described previously [22].

Author Manuscript Author Manuscript Author Manuscript Author Manuscript

2.2. Computational cardiac models of biventricular hearts

Subject-specific computational models were created for each subject using data acquired at the termination point (week 16) and simulate function at that point in time. The creation and validation of precise subject-specific computational swine models of the heart have been detailed extensively in our prior work [21], and are briefly recounted here. Our computational models include geometric precise representations of the ventricular structure, the fibrotic tissue, and solidified hydrogel injections extracted from *ex vivo* segmentation of high-resolution MRI (Fig. 2 A–B). We incorporate myofiber orientations throughout the model (Fig. 2 C) extracted from diffusion tensor magnetic resonance imaging (DTMRI) data, which accurately captures the underlying tissue structure in the heart [24].

2.3. Passive and active myocardium

The passive material response of the cardiac tissue uses an anisotropic hyperelastic formulation proposed by Holzapfel and Ogden [25].A modification in the isochoric part of the strain energy density Ψ_{iso}, was introduced [21], allowing for the description of homogenized, pathological tissue:

$$\Psi_{iso} = \frac{\bar{a}}{2b} e^{b(I_1 - 3)} + \sum_{i=f,s} \frac{\bar{a}_i}{2b_i} \left\{ e^{b_i (I_{4i} - 1)^2} - 1 \right\} + \frac{\bar{a}_{fs}}{2b_{fs}} \left\{ e^{b_{fs} (I_{8fs})^2} - 1 \right\}, \tag{1}$$

$$\Psi_{vol} = \frac{1}{D} \left(\frac{J^2 - 1}{2} - \ln(J) \right) \tag{2}$$

where the new parameters $\bar{a}$, $\bar{a}_i$ and $\bar{a}_{fs}$ govern the homogenization of healthy and pathological tissue using a scalar parameter h representing the volume fraction of tissue health bound between values [0,1]. For example $\bar{a}_i$ is defined in the following manner:

$$\bar{a}_i = a_i [h + (1 - h) p] . \tag{3}$$

Here, h governs the health of the material point and p scales the passive response according to pathology. Note that at $h = 1$, i.e. the material point is entirely healthy, $\bar{a}_i = a_i$.The parameters $\bar{a}$ and $\bar{a}_{fs}$ are defined similarly using h, p, a and a_{fs}.The field variable, h, is determined *a priori* from the mapping of the segmented infarcted tissue and processed as a regionally varying field, continuous over the domain for all subjects (Fig. 3). This process is illustrated in the supplementary Fig. S2. The value for p, which determines the relative stiffness of infarcted regions, was determined from the literature. Multiple studies have quantified infarct stiffness which provides bounds of 2–10 times [26–29] as stiff as remote non-infarcted tissue. Recently, McGarvey, Mojsejenko [28] quantify the *in vivo* stiffness of infarct and remote tissue of porcine subjects. They report their results in the fiber and cross-fiber direction and include data for up to 12 weeks following occlusion. Using the average ratio of these results at 12 weeks for infarcted and remote tissue in both direction, we determine a value for $p = 4.56$.

Author Manuscript Author Manuscript Author Manuscript Author Manuscript

Eq. (1) is now defined through the eight original material parameters a, b, a_f, b_f, a_s, b_s, a_{fs}, b_{fs}, parameters relating to pathology h and p, and four strain invariants I_1, I_{4f}, I_{4s} and I_{8fs}. These strain invariants are derived from the isochoric right Cauchy-Green tensor,

$$\overline{\boldsymbol{C}} = \overline{\boldsymbol{F}}^T\overline{\boldsymbol{F}} = J^{-2/3}\boldsymbol{C} = J^{-2/3}\boldsymbol{F}^T\boldsymbol{F} \tag{4}$$

where **F** is the deformation gradient, J is the determinant of the deformation gradient, $J = \det(\boldsymbol{F})$ and $\overline{\boldsymbol{F}}$ is the isochoric part of the deformation gradient such that

$$\overline{\boldsymbol{F}} = J^{-1/3}\boldsymbol{F} \text{ and } \det(\overline{\boldsymbol{F}}) = 1. \tag{5}$$

The expression of these strain invariants can now be defined as:

$$I_1 = tr(\overline{\boldsymbol{C}}),\ I_{4f} = \boldsymbol{f}_0 \cdot \left(\overline{\boldsymbol{C}}\boldsymbol{f}_0\right),\ I_{4s} = \boldsymbol{s}_0 \cdot \left(\overline{\boldsymbol{C}}\boldsymbol{s}_0\right),\ I_{8fs} = \boldsymbol{f}_0 \cdot \left(\overline{\boldsymbol{C}}\boldsymbol{s}_0\right) \tag{6}$$

Where $\boldsymbol{f}_0$ and $\boldsymbol{s}_0$ are orthogonal vectors in the fiber and sheet direction in the reference configuration. Eq (2) is defined through J and a penalty term D, which is a multiple of the bulk modulus ($D = 2/K$). For deformation that perfectly preserves volume, $J = 1$. This passive material model ensures that the material exhibits the well-documented exponential and anisotropic response to strain [30–32] while enforcing incompressibility.

The description of our time-varying elastance model of active force development [33] is specified as:

$$T_a(t,l) = T_{MAX}\frac{Ca_0^2}{Ca_0^2 + ECa_{50}^2(l)}\frac{(1-\cos(\omega(t,l)))}{2}h \tag{7}$$

where T_{max}, the maximum allowable active tension, is multiplied with a term governing the calcium concentration, and a term governing the timing of contraction. Both terms depend on sarcomere length l, which in turn depends on the strain in the fiber direction. Finally, the entire expression is multiplied by h, to ensure tissue contractility is directly proportional to tissue health. This ensures contractile force is zero at the material point of fully infarcted tissue. The active tension generated from this representation conforms well with experimental studies [33] and captures length-dependent effects such as Frank Starling's Law [34, 35].

We consider the total Cauchy stress to be an additive contribution of passive and active components. The passive Cauchy stress, $\boldsymbol{\sigma_p}$, is given by $\boldsymbol{\sigma_p} = 2J^{-1}\,\boldsymbol{F}\,(\partial\psi/\partial\mathbf{C})\,\mathbf{F}^{\mathrm{T}}$. We consider an active contractile stress in the fiber direction, resulting in a total Cauchy stress in the fiber direction, (i.e. myofiber stress) by combining this with the passive stress state in this direction ($\boldsymbol{\sigma_{pf}}$):

$$\sigma_f = \sigma_{pf} + T_a\boldsymbol{f} \otimes \boldsymbol{f}_0 \tag{8}$$

Author Manuscript Author Manuscript Author Manuscript Author Manuscript

Biaxial investigations on actively contracting rabbit myocardium revealed significant stress development in the cross-fiber direction [36].This has motivated computational efforts to consider a proportion of the active stress developed in the myofiber direction to be transferred onto the stress in the sheet direction by a scalar $n_s \in (0, 1)$, such that the total Cauchy stress in the sheet direction is:

$$\boldsymbol{\sigma_s} = \boldsymbol{\sigma_{ps}} + n_s T_a \boldsymbol{s} \otimes \boldsymbol{s}_0 \tag{9}$$

Cardiac material parameters were calibrated for each subject following the detailed methods in our prior work [21] to ensure that each model incorporated orthotropic material behavior consistent with experimental tri-axial shear response [37] that was scaled to replicate the recorded *in vivo* diastolic pressure-volume response [38], and captured the volume and pressure states at end-diastole (ED) and end-systole (ES). Additional material characterization was incorporated for the description of the solidified alginate injections in the HFI subjects as described in Section 2.4

2.4. Alginate hydrogel

The precise geometric representations of the alginate hydrogel injections extracted from high resolution ex-vivo imaging coincide with the orientation, placement and retained volume of each injection applied to each subject in the HFI group. A compressible Neo-Hookean constitutive law is used to describe the material behavior of the solidified alginate hydrogel:

$$\Psi_{gel} = \frac{\mu}{2}(I_1 - 3) + \frac{K}{2}(J - 1)^2, \tag{10}$$

with new material parameters μ and K being the shear and bulk moduli respectively. Material response for the alginate hydrogel has been previously characterized [23].Using this experimental data and assuming near incompressibility, we calibrated the Neo-hookean material response, which resulted in material parameters $\mu = 8.9$ kPa and $K = 887.0$ kPa (equivalent to a Poisson's ratio $\nu = 0.495$).

2.5. Coupled circulatory models

The model of each heart couples lumped circulatory systems, which remain purely passive, to the high-fidelity geometric representation of the pumping mechanical heart (Fig. 2 D). The circulatory model incorporates unidirectional fluid exchanges driven by the pressure difference and latent compliance of connected chambers. This creates computationally meaningful representation of the dynamic beating of the heart coupled with the circulatory system. Using Abaqus software (version 6.14, Dassault Systèmes, Providence, RI, USA) and high-performance parallel computing resources, we can solve for hundreds of thousands of variables at every time step, giving a highly detailed predictive model of cardiac function and performance. Cardiac function was simulated for six consecutive cardiac cycles to ensure converged solutions were achieved. All values and results reported in the following sections correspond to the final and converged solution.

Author Manuscript Author Manuscript Author Manuscript Author Manuscript

Collectively, these methods allow creation of simulated LV pressure-volume loops that coincide with *in vivo* recorded measurements at ED and ES for each swine. To account for the different chamber sizes due to dilation, volume measurements were normalized as a percentage of LV ED volume for the representation of pressure-volume loops.

2.6. Histological measurement of sarcomere lengths

Under deep anesthesia (isoflurane 5%), the heart was arrested in diastole with a saturated solution of potassium chloride via the jugular vein to assure a relaxed state of sarcomeres. The heart was transported to the lab in cold saline solution for immediate fixation with buffered formalin (Carson-Millonig formulation).

Myocardial samples from the LV free wall and the septum were obtained using a biopsy punch (5mm diameter) from HFC and HFI subjects. From the HFI subjects, LV free wall samples were obtained from the middle regions between the solidified injections. The sample was observed under light microscopy to orient the longitudinal axis of the myocardial fiber parallel to the bottom of the embedding block and parallel to the blade of the cryostat machine during sectioning. Sections of 7 μm thickness were cut using a clinical cryostat (Leica CM1850), mounted on glass slides, and incubated with Wheat Germ Agglutinin, Alexa Fluor® 488 Conjugate (Invitrogen) for cardiomyocyte boundary determination, and with Anti-Sarcomeric Alpha Actinin as the primary antibody and Donkey anti-Mouse IgG (H + L) Highly Cross-Adsorbed Secondary Antibody, Alexa Fluor R 546 (Thermo Fisher), for sarcomere length determination. Fig. 4 shows a representative image of the histological preparation used to determine sarcomere length. Non-repeating fields were surveyed under fluorescence microscopy (Nikon TE-DH100W) for cardiomyocytes in their longitudinal axis, with no tears or sectioning artifacts. Microphotographs were taken using a 20x lens to determine myocyte length and diameter, and a 60x lens for sarcomere length and number. Measurements were obtained using ImageJ software. Sarcomere length was measured by obtaining the distance between two Z-discs at 600x magnification. A total of 539 sarcomeres were measured in the HFC group and 586 sarcomeres in the HFI group from 10–15 images per heart for each group.

2.7. Statistical analysis

Data are expressed as mean ± SD unless otherwise stated. The differences between groups were evaluated using analysis of variance (ANOVA) and Student's t-test and considered statistically significant at $p < 0.05$.

3. Results

3.1. Treatment reduced failing LV unloaded cavity volumes

The segmentation techniques allowed creation of high-fidelity representations of unloaded ventricular structures for all 15 swine. Fig. 3 illustrates the geometric segmentation from high resolution MRI to 3D geometric reconstruction, which includes the complex representations of infarcted and border-zone tissue within the ventricular structure. Measurement of the unloaded cavity volumes for the NC, HFC and HFI groups revealed that the untreated HF swine experienced twice the dilation as treated swine compared to the NC

Author Manuscript Author Manuscript Author Manuscript Author Manuscript

group (20.0 vs. 40.9% dilated for HFC vs. HFI). However, the absolute values for these unloaded volumes were 23.54 ± 6.27 (NC), 33.17 ± 8.25 (HFC) and 28.25 ± 6.87 mL (HFI), which were not statistically significant ($p = 0.148$).

3.2. Treatment limits unloaded sarcomere lengths of surrounding myocardium

Histological measurements of sarcomere lengths in the free wall were 5.8% greater for the HFC group than for the HFI group (1.78 ± 0.15 vs. 1.68 ± 0.10 μm, $p<0.001$). To investigate the hypothesis that the injected hydrogel has a regional effect on preventing adverse remodeling, measurements in the septal wall (i.e., a distinct region relatively far from hydrogel injections) were obtained. Sarcomere lengths in the septal wall were the same for the HFC and HFI groups (1.79 ± 0.14 vs. 1.79 ± 0.12 μm, $p = 0.94$), which were also the same for the HFC free wall (1.78 ± 0.15).

Additional histological investigation of the hydrogel-tissue interface showed that the injections solidified as mid-wall implants and always induced a full (360 °) encapsulation with fibrotic tissue, as can be seen in Fig. 5.*Ex vivo* physical examination (i.e., palpation) of the treated hearts indicated that the encapsulated hydrogel was firmly embedded within the tissue.

3.3. Treatment increased failing LV ejection fraction

LV functional outputs compared excellently between *in vivo* and *in silico* results, e.g., stroke volume (SV) was reproduced *in silico* with 99.6% (NC), 99.1% (HFC) and 99.5% (HFI) accuracy. Full functional outputs are presented in Table 1.Additional data on cavity pressures is provided in the supplementary data in Table S1. The mean pressure-volume loops for each group, normalized by ED volume, showed the treated cohort functioning intermediately between the healthy and untreated groups (Fig. 6). Notably, LV ED pressures were less elevated in the treated swine (16.53 vs 12.39 mmHg) (control vs treated), and LV EF was significantly improved when the treated and untreated cohorts were compared (43.9 ± 2.8 vs 34.7 ± 2.7%, $p<0.01$).

3.4. Myofiber strains were substantially reduced in vicinity of solidified hydrogel

Myofiber stress and strain values for each ventricle at ED and at ES were volumetrically averaged (i.e., normalized by element volume) to remove potential mesh artifacts and the mean values in the LV and RV are presented in Table 2 for each group. ED myofiber stress was elevated in the HFC group compared to the NC group (1.9 ± 3.5 vs. 2.3 ± 3.7 kPa) ($p<0.001$), whereas the HFI group had normalized values when compared to the NC group (1.9 vs. 2.0 kPa) as seen in Fig. 7.The most noteworthy finding was that myofiber strains (and corresponding stresses) in the vicinity of the solidified hydrogel were substantially reduced and that this effect was sustained for up to 13 mm away from the material (i.e., the mechanical sphere of influence extends 13 mm volumetrically away from the implant) (Fig. 8).

An additional analysis of strain behavior decomposed into principal directions allowed for consistent tracking of both the myocardium and hydrogel strain. We found that the mean strain in the hydrogel corresponds to the minimum strain value experienced in the

Author Manuscript Author Manuscript Author Manuscript Author Manuscript

myocardium, which also coincides with the myocardial tissue in direct contact with the hydrogel injections (Fig. 8).

For example, the mean values in the hydrogel for the 1st, 2nd and 3rd principal strains were −5.86 ± 6.76, 0.66 ± 2.98 and 7.23 ± 8.64, respectively. These coincide with the principal strains in the myocardium in the direct vicinity of the gel surfaces: −5.87 ± 5.93, 1.21 ± 2.71 and 8.44 ± 10.12 for the 1st, 2nd and 3rd principal strains respectively. These are the minimum strains in the LV, which increase in magnitude within the tissue as the distance from the hydrogel increases (Fig. 9).

4. Discussion

The major finding of this study—that myofiber strains (and corresponding stresses) in the vicinity of the solidified hydrogel were substantially reduced and that this effect was sustained for up to 13 mm away from the material—suggests that a series of circumferential hydrogel injections prevent dilation of the ventricle. Within eight weeks of treatment and measured in the unloaded *ex vivo* state, swine injected with intra-myocardial hydrogel had less elongated sarcomeres, by approximately 8%, which in turn resulted in LV cavities 20% smaller than those of untreated swine. This difference provides an objective quantitative measurement of ventricle dilation (and its attenuation) independent of *in vivo* ventricular loading.

4.1. Mechanism of action of hydrogel implants

The current mechanism of action of hydrogel implants is thought to be stress reduction, wherein the acute effect of the injections is to unload the adjacent myocytes, i.e., reduce the stress on myocytes as the hydrogel takes up the load [11, 13, 16].The bulking of wall thickness (based primarily on the original canine studies with micro-embolization to induce HF [13]) was thought to reduce mean wall stress through Laplace's law. Our studies, which use a novel large-artery-occlusion model with coils to induce HF, have not confirmed the bulging of LV wall. As noted in our prior studies on the same swine presented here, treated swine experienced improvements in EF, stroke volume, and wall thickness when measured *in vivo* [15].When measured *ex vivo* (i.e., in the unloaded state), wall thickness did not significantly differ between treated and untreated swine [22].The volume of injected hydrogel is $<3\%$ of wall volume [22], and even if this amount *did* increase wall thickness, it would likely have a very small effect. Rather, we believe the mechanism of action stems from a chronic effect where the hydrogel stimulates the genesis of fibrotic encapsulation to restrain or "glue" the adjacent myocytes around the entire surface of the implanted hydrogel. Combined with the circumferential pattern of injections, this creates an effective LV mid-wall constraint (LVMC) to prevent LV dilation, which in turn reduces the stress on myocytes. This is confirmed by the detailed principal strain analysis based on proximity to the gel surfaces, which shows that the mean strain in the solidified gel injections coincides with the minimum strains experienced in the myocardium. These minimum strain values occur directly at the gel-tissue interface. The strain results show the variance around mean values increasing as distance from the injectates increases (Figs. 8 and 9). This illustrates

Author Manuscript Author Manuscript Author Manuscript Author Manuscript

uniformity of mechanics at the gel-tissue interface and conversely illustrates the heterogeneity of tissue mechanics as larger regions are lumped together.

A hypothesis of LVMC consistently explains our current and previous findings. The mitigation of dilation in the treated cohort leads to relative gains in functional performance. Within eight weeks of treatment, EF was almost 10% higher (absolute terms) in the treated swine: 43.9% ±2.8% vs. 34.7% ± 2.7% (HFI vs. HFC; $p < 0.01$). Treated swine experienced lower pressures at ED, and larger ejection fractions and greater pressures during systole, which can be seen qualitatively in Fig. 6. Collectively these results suggest that treatment with hydrogel injections mitigates the degradation of systolic performance following ischemic HF. Comparative improvements in systolic performance and lower ED pressures would explain why the same subjects experience increased wall thickness *in vivo* [15] and not *ex vivo* [22].These are also features of another highly sought-after target of HF treatment: the normalization of dysfunctional, yet viable, myocardium present in most cases of heart failure [8, 39].

The untreated LV tissue clearly experienced permanent deformation that propagates down to the micro-scale, as shown by our findings that sarcomere lengths are elongated in the HFC group, and in the untreated septal wall of the HFI group. This is critical in soft tissues because mechanical behavior on the macro-scale is linked to the state of micro-scale constituents; e.g., passive compliance of myocardial tissue is often explained by undulating fiber constituents acting on the micro-scale that contribute to stiffness when they are elongated and thus engaged [40,41].

The hydrogel, while able to deform, experiences less strain than the surrounding myocardium. Once present, it may anchor and support the surrounding tissue. An additional benefit is that these gels, once solidified, cannot undergo remodeling in the critical early stages following infarction. This ensures that the region of ventricular wall space the hydrogel occupies (together with the fibrotic capsule) is not susceptible to remodeling, further dilation or infarct expansion. This is prominently illustrated in Fig. 3, whereby the progression of adverse remodeling dramatically affected the infarct expansion and wall thinning in the LV free wall of some of the untreated subjects. In contrast, all of the treated subjects retain wall thickness and show large regions of viable, healthy tissue within the LV free wall. The ability of the hydrogel to deform avoids adverse secondary outcomes that might restrict the LV's passive function.

ED stress values in the treated group were similar to those in the NC group, whereas in the untreated group, they were elevated by 23% ((1.9 vs. 2.3 kPa) (HFI vs. HFC), $p < 0.01$). Reduction in wall stress following hydrogel injection therapy is a consistent finding in prior studies [18, 23, 42–48].Additionally, improvement in EF (and other functional outputs) following intra-myocardial hydrogel injection therapy is also a common finding in animal studies over the last decade, providing an overwhelming body of evidence to support that the therapy improves function [49].Disappointingly, this benefit to cardiac function has not been demonstrated in clinical trials [20,50].The lack of clinical translation may be better explained now that the mechanism of action has been better elucidated. The primary therapeutic benefit from acellular hydrogel injection stems from the structural support (i.e.,

Author Manuscript Author Manuscript Author Manuscript Author Manuscript

mid-wall constraint) that attenuates further adverse remodeling. Both control and treated patients in the AUGMENT-HF trial [20] had no statistically significant change in EF, which can be explained if these patients had already reached a stable state of cardiac impairment; i.e., hydrogel injections do not directly improve systolic performance. Rather, they attenuate the loss of function, and for these patients its application may have been too late. Any systolic improvement, as was seen in our own animal studies immediately following injection therapy [15], is likely due to recovery of viable myocardium facilitated by the favorable conditions provided by LVMC. This would imply that if a new criterion was introduced that limits selection to patients actively undergoing LV remodeling, the efficacy seen in pre-clinical studies may translate better to patients. There is substantial evidence that hydrogel injections attenuate the remodeling process on the macro- (unloaded cavity volumes) and micro- (sarcomere lengths) scale. The proposed mechanism of action (LVMC) is the conceptual conclusion drawn from these key results; i.e., the reduced strains seen in our computational models and the sum of evidence in our prior studies of the same subjects. Computational models informed by state-of-the-art imaging produce a scientific modality of investigation that is better than the sum of its parts. As pointed out in our recent modeling methods paper [21], the degree of animal-specificity included in all 15 of the models in the present study represents a milestone for modeling efforts that captures realism of the whole heart. This has provided us the means to interrogate the underlying mechanics of a promising therapy and expand the understanding surrounding treatment efficacy.

4.2. Further research

Further clinical experimentation and computational research is needed to validate this LVMC model. A chemical inhibition of the encapsulation of the hydrogel, creating an “untethered” control therapy to test the LVMC hypothesis, is warranted in future studies. Additionally, the technique we developed here could be used with non-inert biopolymers to assess what fraction of their mechanism of action is mechanically based versus other bioactive signaling.

Our studies support the novel concept that the injection of small amounts of inert hydrogel into the LV free-wall, with or without CABG, is effective for preventing dilation (i.e., decreases strain and myofiber stress) and consequently improves LV function. Moreover, if the hydrogel can be delivered percutaneously rather than via the currently used open-chest procedure, this therapy may become routine for HF treatment. A minimally invasive procedure would be in the best interest of this patient population; i.e., one that cannot tolerate general anesthesia and surgery, and it would be significantly more cost-effective than surgery.

4.3. Limitations

This research has several limitations. Primarily, the computational models exclude the atria and the heart valves. This limits our ability to predict the effect of treatment on atrioventricular interactions, such as flow regurgitation. Secondly, the determination of pathological scaling, p, is an oversimplification. Ideally these values would be determined experimentally from the subjects they are applied to. Additionally, end-systolic stresses were higher in treated subjects than in either normal or untreated subjects (Table 2). Because the

Author Manuscript Author Manuscript Author Manuscript Author Manuscript

variance in the data was large (SD = ± 25.7 kPa) and peak systolic pressure in the treated subjects remained within normal values, it is unclear if this finding is meaningful without further study. Large variance of data in general is a further limitation of this study that could be improved by increasing the number of animals studied in future work. This research could be further improved with more detailed investigations into the underlying cellular and molecular remodeling process. This remains an area of ongoing investigation.

5. Conclusions

Our findings suggest that solidified alginate hydrogel material acts as an LV mid-wall constraint in swine that significantly reduces adverse LV remodeling compared to untreated HF controls without causing negative secondary outcomes to cardiac function. We hypothesize that the encapsulation of the gels provides additional support, facilitated by the tethering of the gels to the surrounding tissue.

Supplementary Material

Refer to Web version on PubMed Central for supplementary material.

Acknowledgments

The authors thank Pamela Derish in the Department of Surgery, University of California San Francisco for proofreading the manuscript.

Funding

This work was supported by NIH grants R01-HL-077921, R01-HL-118627 and U01-HL-119578. Further financial support was provided by the Oppenheimer Memorial Trust (OMT) and the National Research Foundation (NRF) of South Africa. Opinions expressed and conclusions arrived at are those of the authors and are not necessarily to be attributed to the NRF or OMT.

References

[1]. Benjamin EJ, Virani SS, Callaway CW, Chamberlain AM, Chang AR, Cheng S, et al., Heart disease and stroke statistics—2018 update: a report from the american heart association, Circulation 137 (2018) e67–e492. [PubMed: 29386200]

[2]. Mozaffarian D, Benjamin EJ, Go AS, Arnett DK, Blaha MJ, Cushman M, et al., Heart disease and stroke statistics—2016 update a report from the American heart association, Circulation (2015) CIR. 0000000000000350.

[3]. Wenk JF, Klepach D, Lee LC, Zhang Z, Ge L, Tseng EE, et al., First evidence of depressed contractility in the border zone of a human myocardial infarction, Ann. Thorac. Surg 93 (2012) 1188–1193. [PubMed: 22326127]

[4]. ElOakley RM, Yonan NA, Simpson BM, Deiraniya AK, Extended criteria for cardiac allograft donors: a consensus study, J. Heart Lung. Transplant 15 (1996) 255–259. [PubMed: 8777208]

[5]. Keck BM, Bennett LE, Fiol BS, Daily OP, Novick RJ, Hosenpud JD World-wide thoracic organ transplantation: a report from the UNOS/ISHLT international registry for thoracic organ transplantation. Clin Transpl. 1995:35–48. [PubMed: 8794253]

[6]. Hutchins GM, Bulkley BH, Infarct expansion versus extension: two different complications of acute myocardial infarction, Am. J. Cardiol 41 (1978) 1127–1132. [PubMed: 665522]

[7]. Mann DL, Mechanisms and models in heart failure: a combinatorial approach, Circulation: Citeseer (1999).

Author Manuscript Author Manuscript Author Manuscript Author Manuscript

[8]. Brown DA, Perry JB, Allen ME, Sabbah HN, Stauffer BL, Shaikh SR, et al., Expert consensus document: mitochondrial function as a therapeutic target in heart failure, Nat. Rev. Cardiol 14 (2017) 238–250. [PubMed: 28004807]

[9]. Senni M, Gavazzi A, Gheorghiade M, Butler J, Heart failure at the crossroads: moving beyond blaming stakeholders to targeting the heart, Eur. J. Heart Fail 17 (2015) 760–763. [PubMed: 26179815]

[10]. Plotkin M, Vaibavi SR, Rufaihah AJ, Nithya V, Wang J, Shachaf Y, et al.,The effect of matrix stiffness of injectable hydrogels on the preservation of cardiac function after a heart attack, Biomaterials 35 (2014) 1429–1438. [PubMed: 24268664]

[11]. Kadner K, Dobner S, Franz T, Bezuidenhout D, Sirry MS, Zilla P, et al., The beneficial effects of deferred delivery on the efficiency of hydrogel therapy post myocardial infarction, Biomaterials 33 (2012) 2060–2066. [PubMed: 22153866]

[12]. Dobner S, Bezuidenhout D, Govender P, Zilla P, Davies N, A synthetic non-degradable polyethylene glycol hydrogel retards adverse post-infarct left ventricular remodeling, J. Card Fail 15 (2009) 629–636. [PubMed: 19700140]

[13]. Sabbah HN, Wang M, Gupta RC, Rastogi S, Ilsar I, Sabbah MS, et al., Augmentation of left ventricular wall thickness with alginate hydrogel implants improves left ventricular function and prevents progressive remodeling in dogs with chronic heart failure, JACC Heart Fail 1 (2013) 252–258. [PubMed: 23998003]

[14]. Leor J, Tuvia S, Guetta V, Manczur F, Castel D, Willenz U, et al., Intracoronary injection of in situ forming alginate hydrogel reverses left ventricular remodeling after myocardial infarction in swine, J. Am. Coll. Cardiol 54 (2009) 1014–1023. [PubMed: 19729119]

[15]. Choy JS, Leng S, Acevedo-Bolton G, Shaul S, Fu L, Guo X, et al., Efficacy of intramyocardial injection of ALGISYL-LVR for the treatment of ischemic heart failure in swine, Int. J. Cardiol 255 (2018) 129–135. [PubMed: 29425550]

[16]. Rodell CB, Lee ME, Wang H, Takebayashi S, Takayama T, Kawamura T, et al., Injectable shear-thinning hydrogels for minimally invasive delivery to infarcted myocardium to limit left ventricular remodeling, Circ. Cardiovasc Interv 9 (2016) e004058. [PubMed: 27729419]

[17]. Gaffey AC, Chen MH, Trubelja A, Venkataraman CM, Chen CW, Chung JJ, et al., Delivery of progenitor cells with injectable shear-thinning hydrogel maintains geometry and normalizes strain to stabilize cardiac function after ischemia, J. Thorac. Cardiovasc. Surg 157 (2019) 1479–1490. [PubMed: 30579534]

[18]. Lee LC, Wall ST, Klepach D, Ge L, Zhang Z, Lee RJ, et al., Algisyl-lvr with coronary artery bypass grafting reduces left ventricular wall stress and improves function in the failing human heart, Int. J. Cardiol 168 (2013) 2022–2028. [PubMed: 23394895]

[19]. Lee RJ, Hinson A, Bauernschmitt R, Matschke K, Fang Q, Mann DL, et al., The feasibility and safety of ALGISYL-LVR™ as a method of left ventricular augmentation in patients with dilated cardiomyopathy: initial first in man clinical results, Int. J. Cardiol 199 (2015) 18–24. [PubMed: 26173169]

[20]. Mann DL, Lee RJ, Coats AJ, Neagoe G, Dragomir D, Pusineri E, et al., One-year follow-up results from augment-hf: a multicentre randomized controlled clinical trial of the efficacy of left ventricular augmentation with algisyl in the treatment of heart failure, Eur. J. Heart Fail 18 (2016) 314–325. [PubMed: 26555602]

[21]. Sack KL, Aliotta E, Ennis DB, Choy JS, Kassab GS, Guccione JM, et al., Construction and validation of subject-specific biventricular finite-element models of healthy and failing swine hearts from high-resolution DT-MRI, Front Physiol 9 (2018) 539. [PubMed: 29896107]

[22]. Sack K, Aliotta E, Choy J, Ennis D, Davies N, Franz T, et al., Effect of intra-myocardial ALGISYL-LVR™ injectates on fibre structure in porcine heart failure, J. Mech. Behav. Biomed. Mater 87 (2018) 172–179. [PubMed: 30071487]

[23]. Wenk JF, Wall ST, Peterson RC, Helgerson SL, Sabbah HN, Burger M, et al., A method for automatically optimizing medical devices for treating heart failure: designing polymeric injection patterns, J. Biomech. Eng 131 (2009) 121011. [PubMed: 20524734]

Author Manuscript Author Manuscript Author Manuscript Author Manuscript

[24]. Kung GL, Nguyen TC, Itoh A, Skare S, Ingels NB Jr.,Miller DC , et al., The presence of two local myocardial sheet populations confirmed by diffusion tensor MRI and histological validation, J. Magn. Reson. Imaging 34 (2011) 1080–1091. [PubMed: 21932362]

[25]. Holzapfel GA, Ogden RW, Constitutive modelling of passive myocardium: a structurally based framework for material characterization, Philos. Trans. A Math. Phys. Eng. Sci 367 (2009) 3445–3475. [PubMed: 19657007]

[26]. Gupta KB, Ratcliffe MB, Fallert MA, Edmunds LH Jr., Bogen DK, Changes in passive mechanical stiffness of myocardial tissue with aneurysm formation, Circulation 89 (1994) 2315–2326. [PubMed: 8181158]

[27]. Mojsejenko D, McGarvey JR, Dorsey SM, Gorman JH 3rd, Burdick JA, Pilla JJ, et al., Estimating passive mechanical properties in a myocardial infarction using mri and finite element simulations, Biomech. Model Mechanobiol 14 (2015) 633–647. [PubMed: 25315521]

[28]. McGarvey JR, Mojsejenko D, Dorsey SM, Nikou A, Burdick JA, Gorman JH, et al., Temporal changes in infarct material properties: an in vivo assessment using magnetic resonance imaging and finite element simulations, Ann. Thorac. Surg 100 (2015) 582–589. [PubMed: 26095107]

[29]. Connelly CM, Vogel WM, Wiegner AW, Osmers EL, Bing OH, Kloner RA, et al., Effects of reperfusion after coronary artery occlusion on post-infarction scar tissue, Circ. Res 57 (1985) 562–577. [PubMed: 4042284]

[30]. Demer LL, Yin FC, Passive biaxial mechanical properties of isolated canine myocardium, J. Physiol 339 (1983) 615–630. [PubMed: 6887039]

[31]. Hunter PJ, McCulloch AD, ter Keurs HE, Modelling the mechanical properties of cardiac muscle, Prog. Biophys. Mol. Biol 69 (1998) 289–331. [PubMed: 9785944]

[32]. Dokos S, Smaill BH, Young AA, LeGrice IJ, Shear properties of passive ventricular myocardium, Am. J. Physiol. Heart Circ. Physiol 283 (2002) H2650–H2659. [PubMed: 12427603]

[33]. Guccione JM, McCulloch AD, Mechanics of active contraction in cardiac muscle: part i-constitutive relations for fiber stress that describe deactivation, J. Biomech. Eng 115 (1993) 72–81. [PubMed: 8445901]

[34]. Holmes JW, Hunlich M, Hasenfuss G, Energetics of the frank-starling effect in rabbit myocardium: economy and efficiency depend on muscle length, Am. J. Physiol. Heart Circ. Physiol 283 (2002) H324–H330. [PubMed: 12063305]

[35]. Solaro RJ, Mechanisms of the frank-starling law of the heart: the beat goes on, Biophys. J 93 (2007) 4095–4096. [PubMed: 17766360]

[36]. Lin D, Yin F, A multiaxial constitutive law for mammalian left ventricular myocardium in steady-state barium contracture or tetanus, J. Biomech. Eng 120 (1998) 504–517. [PubMed: 10412422]

[37]. Sommer G, Schriefl AJ, Andrä M, Sacherer M, Viertler C, Wolinski H, et al., Biomechanical properties and microstructure of human ventricular myocardium, Acta Biomater 24 (2015) 172–192. [PubMed: 26141152]

[38]. Klotz S, Hay I, Dickstein ML, Yi GH, Wang J, Maurer MS, et al., Single-beat estimation of end-diastolic pressure-volume relationship: a novel method with potential for noninvasive application, Am. J. Physiol. Heart Circ. Physiol 291 (2006) H403–H412. [PubMed: 16428349]

[39]. Bayeva M, Sawicki KT, Butler J, Gheorghiade M, Ardehali H, Molecular and cellular basis of viable dysfunctional myocardium, Circ. Heart Fail 7 (2014) 680–691. [PubMed: 25028350]

[40]. Holzapfel GA, Biomechanics of soft tissue, Handb. Mater. Behav. Models 3 (2001) 1049–1063.

[41]. Kassab GS, Sacks MS, Structure-Based Mechanics of Tissues and Organs, Springer, 2016.

[42]. Wall ST, Walker JC, Healy KE, Ratcliffe MB, Guccione JM, Theoretical impact of the injection of material into the myocardium: a finite element model simulation, Circulation 114 (2006) 2627–2635. [PubMed: 17130342]

[43]. Wenk JF, Eslami P, Zhang Z, Xu C, Kuhl E, Gorman JH, et al., A novel method for quantifying the in-vivo mechanical effect of material injected into a myocardial infarction, Ann. Thorac. Surg 92 (2011) 935–941. [PubMed: 21871280]

[44]. Legner D, Skatulla S, Bewu JM, Rama RR, Reddy BD, Sansour C, et al., Studying the influence of hydrogel injections into the infarcted left ventricle using the element-free galerkin method, Int. J. Numer. Method Biomed. Eng 30 (2014) 416–429. [PubMed: 24574184]

Author Manuscript Author Manuscript Author Manuscript Author Manuscript

[45]. Kichula ET, Wang H, Dorsey SM, Szczesny SE, Elliott DM, Burdick JA, et al., Experimental and computational investigation of altered mechanical properties in myocardium after hydrogel injection, Ann. Biomed. Eng 42 (2014) 1546–1556. [PubMed: 24271262]

[46]. Dorsey SM, McGarvey JR, Wang H, Nikou A, Arama L, Koomalsingh KJ, et al., Mri evaluation of injectable hyaluronic acid-based hydrogel therapy to limit ventricular remodeling after myocardial infarction, Biomaterials 69 (2015) 65–75. [PubMed: 26280951]

[47]. Kortsmit J, Davies NH, Miller R, Zilla P, Franz T, Computational predictions of improved of wall mechanics and function of the infarcted left ventricle at early and late remodelling stages: comparison of layered and bulk hydrogel injectates, Adv. Biomech. Appl 1 (2013) 41–55.

[48]. Miller R, Davies NH, Kortsmit J, Zilla P, Franz T, Outcomes of myocardial infarction hydrogel injection therapy in the human left ventricle dependent on injectate distribution, Int. J. Numer. Method Biomed. Eng 29 (2013) 870–884. [PubMed: 23640777]

[49]. Zhu Y, Matsumura Y, Wagner WR, Ventricular wall biomaterial injection therapy after myocardial infarction: advances in material design, mechanistic insight and early clinical experiences, Biomaterials 129 (2017) 37–53. [PubMed: 28324864]

[50]. Rao SV, Zeymer U, Douglas PS, Al-Khalidi H, White JA, Liu J, et al., Bioabsorbable intracoronary matrix for prevention of ventricular remodeling after myocardial infarction, J. Am. Coll. Cardiol 68 (2016) 715–723. [PubMed: 27515331]

Author Manuscript Author Manuscript Author Manuscript Author Manuscript

Statement of Significance

Heart failure is considered a growing epidemic and hence an important health problem in the US and worldwide. Its high prevalence (5.8 million and 23 million, respectively) is expected to increase by 25% in the US alone by 2030. Heart failure is associated with high morbidity and mortality, has a 5-year mortality rate of 50%, and contributes considerably to the overall cost of health care ($53.1 billion in the US by 2030). Despite positive initial outcomes emerging from preclinical and early clinical investigation of alginate hydrogel injection therapy as a treatment for heart failure, the lack of knowledge concerning the mechanism of action remains a major shortcoming that limits the efficacy of treatment design. To understand the mechanism of action, we combined high-resolution *ex vivo* magnetic resonance imaging and histological data in swine with state-of-the-art subject-specific computational model simulations. The *in silico* models realistically simulated *in vivo* function with $>$99% accuracy and predicted small myofiber strain in the vicinity of the solidified hydrogel that was sustained for up to 13 mm away from the implant. These findings suggest that the solidified alginate hydrogel material acts as a left ventricular mid-wall constraint that significantly reduces adverse LV remodeling compared to untreated heart failure controls without causing negative secondary outcomes to cardiac function. Moreover, if the hydrogel can be delivered percutaneously rather than via the currently used open-chest procedure, this therapy may become routine for heart failure treatment. A minimally invasive procedure would be in the best interest of this patient population; i.e., one that cannot tolerate general anesthesia and surgery, and it would be significantly more cost-effective than surgery.

Author Manuscript Author Manuscript Author Manuscript Author Manuscript

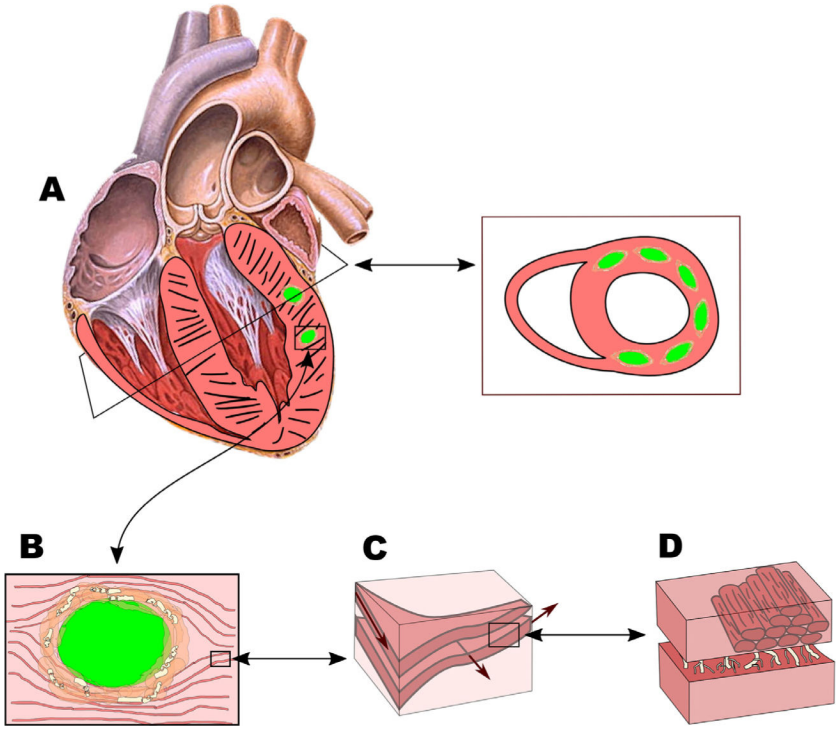

Fig. 1.

Schematic of solidified hydrogel and surrounding fibrotic capsule from macro-to-micro-scale (A-D). The capsule serves to “glue” surrounding myocytes to create a circumferential constraint through the multiple circumferential non-degradable implants. Fig. 1 A-B shows the hydrogel implant and surrounding capsule tightly connecting adjacent sheets and hence providing increased ventricle stiffness in the circumferential direction. Injection pattern consists of 12–14 injections (0.3 ml each) placed in two rows: one above and one below the mid-ventricular plane between the base and the apex (from the anterior to the posterior wall). Fig. 1 C-D shows the orthotropic myocardial ultrastructure.

Author Manuscript Author Manuscript Author Manuscript Author Manuscript

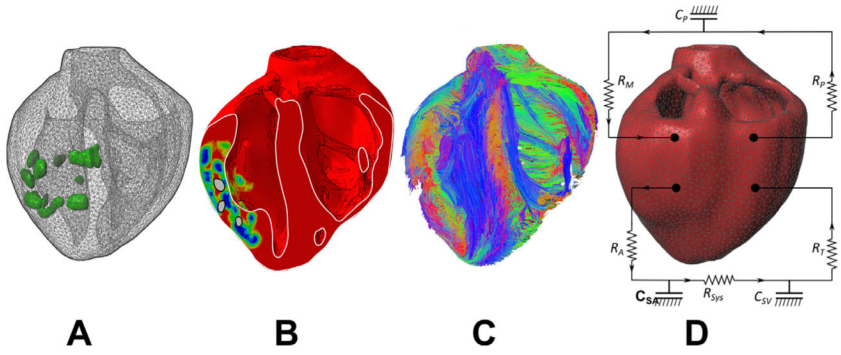

Fig. 2.

High-resolution ex vivo MRI images are processed to segment and construct a meshed geometry of the biventricular structure including the solidified alginate hydrogel injections (A). An additional field variable is introduced throughout the myocardial domain associated with tissue health (B). Healthy tissue (red) and fibrotic tissue (blue) are separated by "border-zone" tissue (rainbow colors). Fiber orientations throughout the myocardium (C) are determined from ex vivo diffusion tensor imaging. Here they are displayed with vector components [x,y,z] corresponding to [red, green, blue]. Preceding geometric information (A-C) is incorporated into the finite element model of the biventricular model coupled to a lumped circulatory model (D).

Author Manuscript Author Manuscript Author Manuscript Author Manuscript

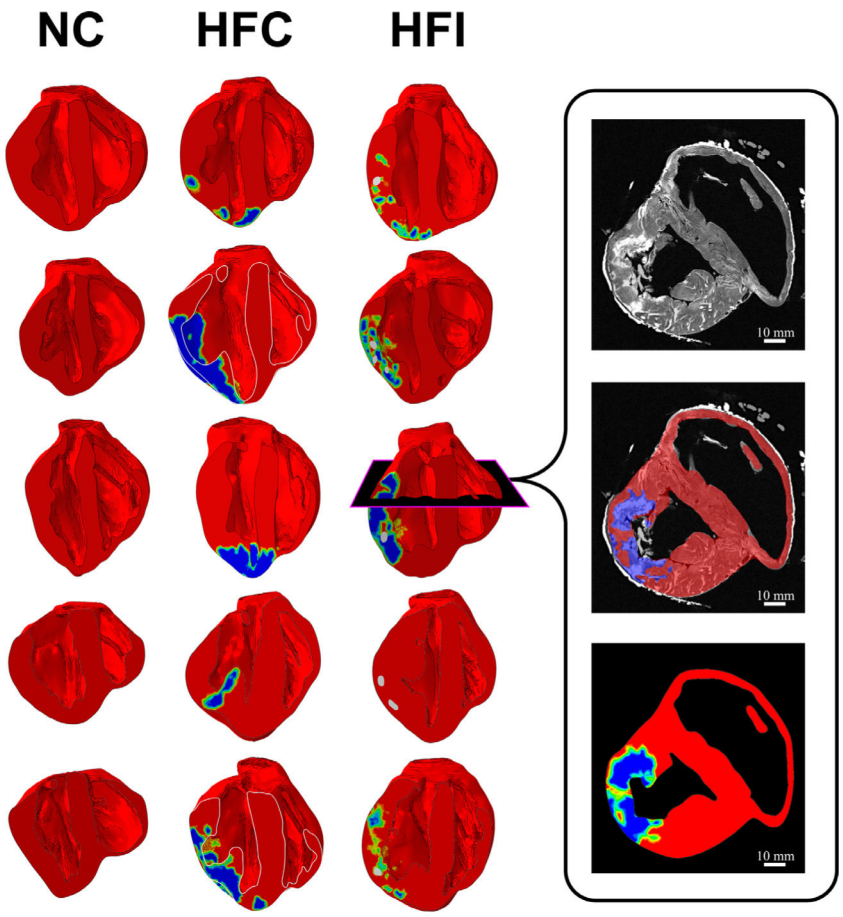

Fig. 3.

Long-axis view of the segmented ventricular structures for the normal control (NC), heart failure control (HFC) and heart failure injected (HFI) for all subjects in this study. Healthy myocardium (red) is separated from fully fibrotic tissue (blue) by border zone (rainbow colors) that transitions smoothly between remote and infarcted regions. Short-axis segmentation of an HFI is shown in the insert panel. The ex vivo MRI image (top) is shown with an overlaid binary segmentation of healthy and fibrotic tissue (middle) and the final interpolated field of the finite element model (bottom). Alginate hydrogel appears as grey.

Author Manuscript Author Manuscript Author Manuscript Author Manuscript

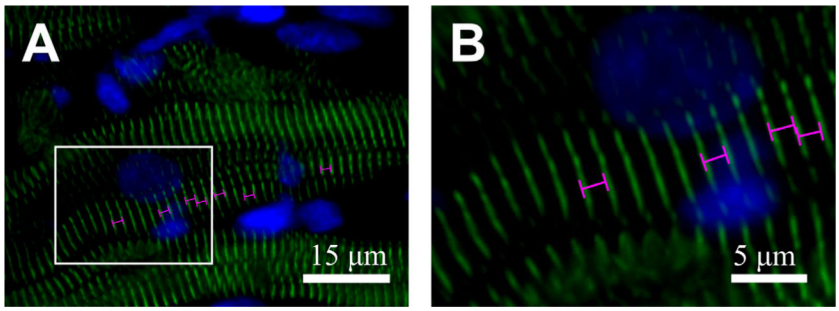

Fig. 4.

A) Representative image of the histological preparation used to determine the sarcomere length. Wheat Germ Agglutinin, Alexa Fluor 488 Conjugate staining, 600 × magnification. Sarcomere measurements were made on a portion of the image where imaging shows no tears, no sectioning artifacts and Z-discs in clear focus. B) Additional magnification of the enclosed region in (A) illustrating the measurements, shown in magenta, which were made from the start of one Z-disc to the start of the next Z-disc.

Author Manuscript Author Manuscript Author Manuscript Author Manuscript

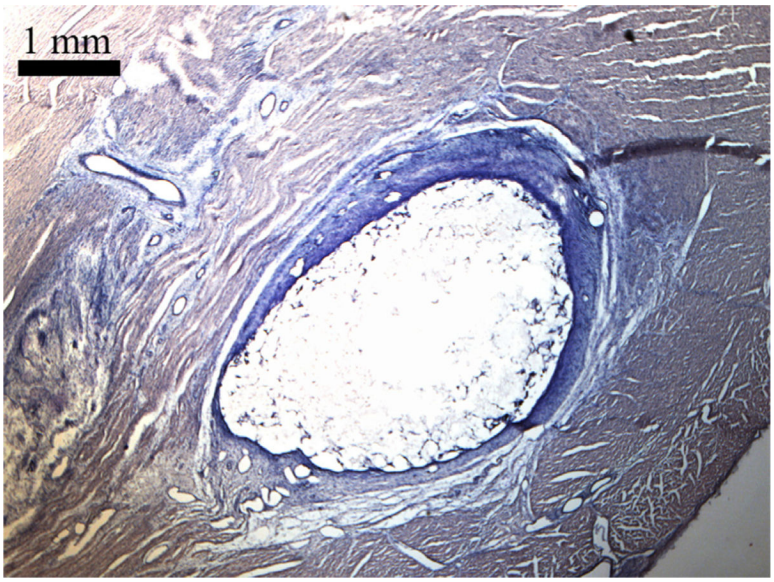

Fig. 5.

Histology of a representative heart from the HFI group. H&E staining with 20 × magnification showing the encapsulated hydrogel implant within the myocardial tissue.

Author Manuscript Author Manuscript Author Manuscript Author Manuscript

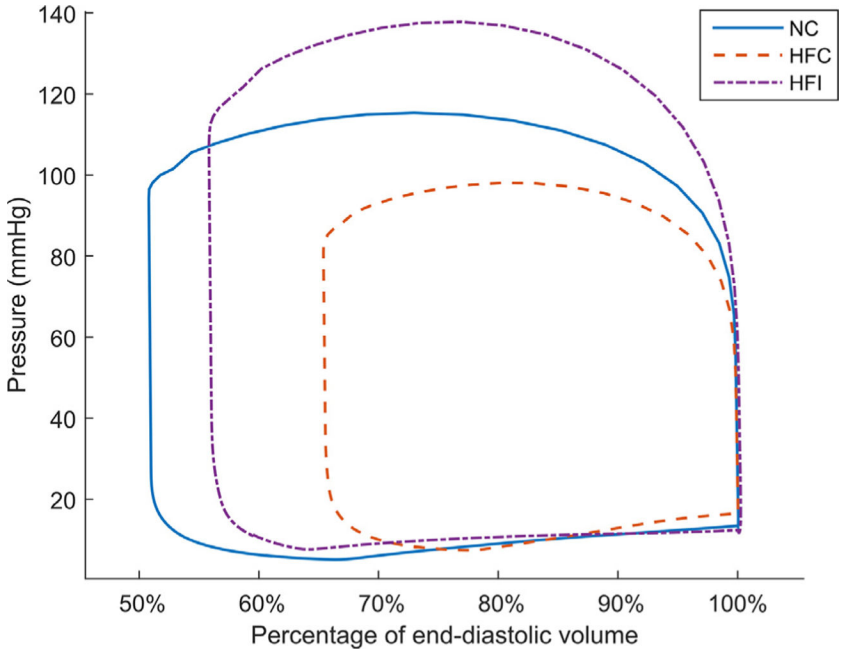

Fig. 6.

Pressure-volume loops for the normal control (NC), heart failure control (HFC) and heart failure treated (HFI) groups. Volume was normalized to the end-diastolic volume for each group.

Author Manuscript Author Manuscript Author Manuscript Author Manuscript

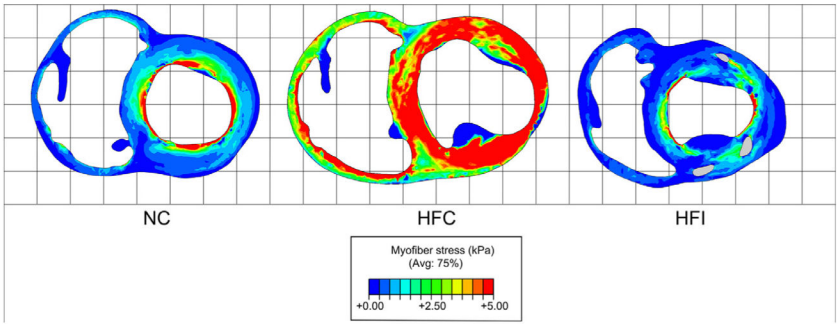

Fig. 7.

End-diastolic myofiber stress values in the short-axis view for representative subjects in the healthy, heart-failure control, and heart failure injected groups.

Author Manuscript Author Manuscript Author Manuscript Author Manuscript

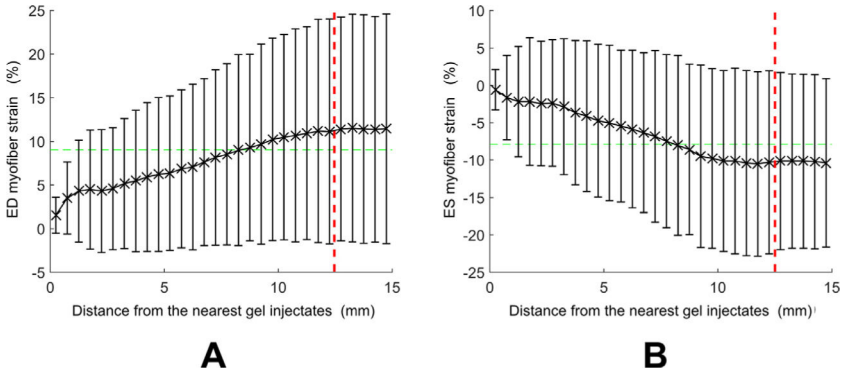

Fig. 8.

Left ventricular (LV) myofiber strains in the heart-failure injected cohort of swine, presented by proximity to hydrogel injection at end-diastole (ED) and end-systole (ES) in (A) and (B) respectively. Error bars correspond to ± SD, global mean LV values are plotted as a dashed green line for each result. Plateau in values marked by a dashed red line.

Author Manuscript Author Manuscript Author Manuscript Author Manuscript

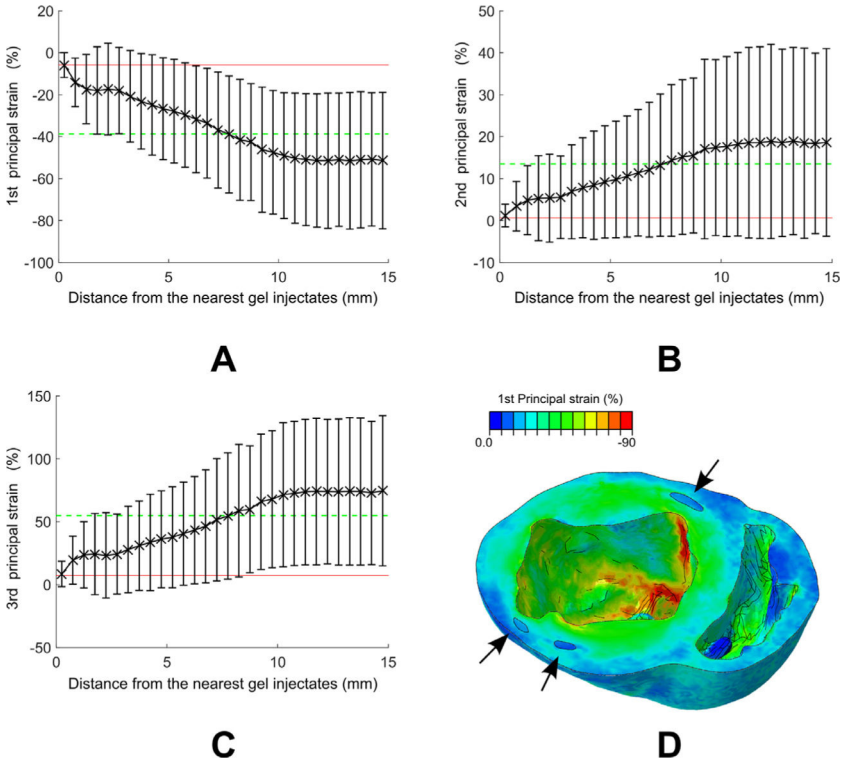

Fig. 9.

End diastole (ED) left ventricular (LV) strains for the heart-failure injected cohort of swine, presented by proximity to hydrogel injection for the first, second and third principal strain direction in (A), (B) and (C) respectively. A mechanical sphere of influence (i.e. volumetrically including all tissue at each radius distance) was considered. Error bars correspond to ± SD, global mean LV values are plotted as a dashed green line for each result, and the hydrogel mean strain values are plotted in a red line. A geometric illustration (D) of the first principal strains in a treated subject's heart (truncated at the mid-myocardium to reveal gel injectates) is shown with black arrows indicating the outline of the solidified injectates.

Author Manuscript Author Manuscript Author Manuscript Author Manuscript

Acta Biomater. Author manuscript; available in PMC 2021 July 15.

Table 1

Functional output values of computational porcine models compared to *in vivo* recorded values.

Subjects	*IN SILICO* LV[≡] EDV[†] (mL)	*IN VIVO* LV EDV (mL)	EDV% of *IN VIVO*	*IN SILICO* LV ESV[‡] (mL)	*IN VIVO* LV ESV (mL)	ESV% of *IN VIVO*	*IN SILICO* SV[††] (mL)	*IN VIVO* SV (mL)	SV% of IN VIVO	*IN SILICO* EF[*](%)	*IN VIVO* EF (%)	EF% of IN VIVO
NC 1	73.9	72.6	102%	35.1	34.7	101%	38.8	37.9	102%	52.5%	52.2%	101%
NC 2	59.8	59.2	101%	26.5	27.0	98%	33.2	32.2	103%	55.6%	54.4%	102%
NC 3	69.4	68.1	102%	36.6	36.0	102%	32.8	32.1	102%	47.2%	47.1%	100%
NC 4	81.0	83.4	97%	42.4	42.9	99%	38.7	40.5	95%	47.7%	48.6%	98%
NC 5	75.0	76.1	99%	41.8	41.5	101%	33.2	34.6	96%	44.3%	45.5%	97%
NC[**] mean	**71.8 ± 7.1**	**71.9 ± 8.1**					**35.3 ± 2.8**	**35.5 ± 3.3**		**49.5 ± 4.1**	**49.6 ± 3.3**	
			99.9 ± 1.9	**36.5 ± 5.7**	**36.4 ± 5.7**	**100.1 ± 1.4**			**99.6 ± 3.4**			**99.8 ± 1.8**
HFC 1	77.3	78.8	98%	52.5	53.8	98%	24.8	25.0	99%	32.0%	31.7%	101%
HFC 2	99.8	103.0	97%	67.7	70.0	97%	32.1	33.0	97%	32.2%	32.0%	100%
HFC 3	96.1	94.8	101%	63.8	62.4	102%	32.2	32.4	99%	33.6%	34.2%	98%
HFC 4	94.9	94.4	101%	58.3	57.9	101%	36.6	36.5	100%	38.6%	38.7%	100%
HFC 5	66.3	67.0	99%	41.7	42.2	99%	24.5	24.8	99%	37.0%	37.0%	100%
HFC[§] mean						**99.2 ± 2.0**	**30.1 ± 4.7**	**30.3 ± 4.7**		**34.7 ± 2.7**	**34.7 ± 2.7**	
	86.9 ± 12.9	**87.6 ± 12.9**	**99.2 ± 1.6**	**56.8 ± 9.1**	**57.3 ± 9.3**				**99.1 ± 1.0**			**99.9 ± 1.0**
HFI 1	110.2	113.3	97%	63.8	65.6	97%	46.4	47.7	97%	42.1%	42.1%	100%
HFI 2	135.5	134.4	101%	70.9	70.0	101%	64.6	64.4	100%	47.7%	47.9%	100%
HFI 3	79.7	77.0	103%	46.2	44.9	103%	33.5	32.1	104%	42.0%	41.7%	101%
HFI 4	124.6	126.5	99%	66.1	68.2	97%	58.5	58.3	100%	46.9%	46.1%	102%
HFI 5	119.8	121.7	98%	71.0	71.0	100%	48.8	50.6	96%	40.7%	41.6%	98%
HFI[//] mean						**99.5 ± 2.3**	**50.4 ± 10.7**	**50.6 ± 11**		**43.9 ± 2.8**	**43.9 ± 2.6**	**100 ± 1.3**
	114 ± 19.0	**114.6 ± 20**	**99.5 ± 2.2**	**63.6 ± 9.1**	**63.9 ± 9.7**				**99.5 ± 2.8**			

[*] EF ejection fraction

[†] EDV = End-diastolic volume

[‡] ESV = End-systolic volume.

[§] HFC = Heart failure control.

Author Manuscript

Author Manuscript

Author Manuscript

Author Manuscript

// HFI = Heart failure injected.

≡ LV = Left ventricle.

** NC = Normal control.

†† SV = Stroke volume.

Author Manuscript

Author Manuscript

Author Manuscript

Author Manuscript

Table 2

End-diastole and end-systole volumetric-averaged mean myofiber stress results for the heart models with converged simulations presented separately for the left and right ventricle.

		Left ventricle	Right ventricle
Stress at end-diastole (kPa)	NC * mean	1.9 ± 3.5	0.9 ± 0.9
	HFC † mean	2.3 ± 3.7	1.5 ± 1.6
	HFI ‡ mean	2.0 ± 4.1	0.6 ± 0.8
Stress at end-systole (kPa)	NC mean	18.0 ± 16.9	19.6 ± 17.7
	HFC mean	17.5 ± 16.7	19.0 ± 15.3
	HFI mean	23.9 ± 25.7	20.3 ± 18.8

* NC Normal control.

† HFC== Heart failure control.

‡ HFI = Heart failure injected.